International Symposium
On Turbulence and Shear Flow
Phenomena (TSFP-9)
June 30 - July 3, 2015 *Melbourne, Australia*

CONSEQUENCES OF SELF-PRESERVATION IN A TURBULENT FAR-WAKE

S. L. Tang
Institute for Turbulence-Noise-Vibration Interaction and Control, Shenzhen Graduate School,
Harbin Institute of Technology, Shenzhen, 518055, P. R. China
School of Engineering, University of Newcastle, NSW 2308, Australia

R. A. Antonia
School of Engineering, University of Newcastle, NSW 2308, Australia
email:robert.antonia@newcastle.edu.au

L. Djenidi
School of Engineering, University of Newcastle, NSW 2308, Australia

Y. Zhou
Institute for Turbulence-Noise-Vibration Interaction and Control, Shenzhen Graduate School,
Harbin Institute of Technology, Shenzhen, 518055, P. R. China

ABSTRACT

On the basis of a two-point similarity analysis, the power-law variations for the different length-scales (e.g. the Taylor microscale, and the Kolmogorov scale) and the velocity scales (e.g. the rms, the Kolmogorov velocity) in the far-wake of a circular cylinder are derived. In particular, an exact relation for estimating the mean turbulent energy dissipation rate $\bar{\varepsilon}$ on the wake axis is obtained. All these relations are supported reasonably well by hot-wire data in the far-wake at a Reynolds number based on the free stream velocity and the cylinder diameter of 2000.

INTRODUCTION

The hypothesis of self-preservation (hereafter denoted SP), which assumes that the flow is governed by a single set of length and velocity scales, has been extensively used to describe the spatial evolution of one-point statistics in the far field of the plane wake. Townsend (1956) was first to carry out a SP analysis in the nominally two-dimensional turbulent wake based on the mean motion equation

$$U\frac{\partial U}{\partial x}+\frac{\partial \overline{u_1u_2}}{\partial y}=\nu\frac{\partial^2 U}{\partial y^2} \qquad (1)$$

where U is the mean velocity in the streamwise direction; $u_i(i=1,2,3)$ is the velocity fluctuations in x, y, and z directions, respectively. While, in theory, SP solutions are independent of the initial conditions, there is a significant amount of evidence which suggests that the state of SP that is reached in the far-wake does depend on the initial conditions (IC), (e.g. Wygnanski *et al.*, 1986; George, 1989; Zhou & Antonia, 1995; Antonia & Mi, 1998; Zhou *et al.*, 1998). The effects of the ICs on SP has been recently reviewed in detail by George (2012) in the more general context of free shear flows. Given this, we only focus on the far-wake of a circular cylinder in this paper. This flow has received a significant amount of attention (e.g. Browne & Antonia, 1986; Antonia & Browne, 1986; Browne *et al.*, 1987; Antonia *et al.*, 1987, 1988; Bisset *et al.*, 1990a,b; Aronson & Löfdahl, 1993; Zhou *et al.*, 2006; Brown & Roshko, 2012).

Exact SP is achieved in a turbulent flow when all statistics scale on one velocity scale and one length scale. This is also reflected in the constancy of R_λ ($=u'\lambda/\nu$; λ is the Taylor microscale, u' is the rms streamwise velocity) as the flow evolves in the streamwise direction since the constancy of R_λ ensures that the ratios between the different length-scales (e.g. the Taylor microscale, and the Kolmogorov scale) and the velocity scales (e.g. the rms, the Kolmogorov velocity) are constant (Burattini *et al.*, 2005; Thiesset *et al.*, 2014). In this case, all the velocity and length scales can be used interchangeably because they all behave similarly. In this paper, we extend the SP analysis of Townsend (1956) to two-point statistics which may provide a deeper insight into the flow details since the evolution of the turbulent structure at a given scale can be assessed. This paper is structured as follows. Details associated with the measurements are

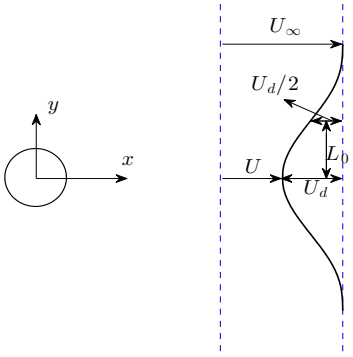

Figure 1. Schematic arrangement and coordinate axis.

described in the next section. Thereafter, we will focus on the SP analysis of the scale-by-scale energy budget equation in the far-wake. Then, experimental support for the results from SP analysis is presented and discussed.

Experimental details

Experiments have been carried out in a non-return blower-type wind tunnel with a square crossection (350 × 350 mm) of 2.4m in length. The inclination of the bottom wall of the working section was adjusted in order to maintain a zero streamwise pressure gradient. The wake is generated by a cylinder (d = 3 mm), which was installed horizontally in the mid-plane and spaning the full width of the working section (Fig. 1). It is located 10 cm downstream of the exit plane of the contraction. This resulted in a blockage of about 0.9% and an aspect ratio of 175. The free-steam velocity U_∞ is 10.6 m/s and the corresponding Reynolds number R_d, based on d and U_∞, is 2000. The measurement locations varied from the near-wake ($x/d = 20$) to the far-wake ($x/d = 600$).

The Wollaston (Pt-10%Rh) hot wire (diameter d_w=2.5 μm) is etched to an active length of about l_w=0.5 mm. The length to diameter ratio of the wire is typically 200. The hot wire is operated with constant-temperature anemometers at an overheat ratio of 1.5. The output signals from the anemometers were passed through buck and gain circuits and low-pass filtered (the cut-off frequency f_c, which was in the range 6300-12500 Hz depending on the transverse position of the probe, was set close to the Kolmogorov frequency $f_\eta = \frac{U}{2\pi\eta}$, where η is the Kolmogorov length scale). The signal is then digitized into a personal computer using a 12 bit analog-to-digital (A/D) converter at a sampling frequency in the range 12600 to 25000 Hz. The record duration, which varied between 100 s and 140 s, is long enough for second- and third-order moments to converge on the basis of criteria proposed by Anselmet *et al.* (1984) and Camussi & Guj (1995).

SP analysis of the scale-by-scale energy budget equation

According to Danaila *et al.* (2001), the scale-by-scale energy budget equation on the axis of a plane far-wake can be given by

$$\begin{array}{l} -\frac{1}{r^2}\int_0^r s^2[U\frac{\partial\overline{\Delta u_i^2}}{\partial x}]ds+\frac{2}{r^2}\int_0^r s^2[-\frac{\partial\overline{u_2\Delta u_i^2}}{\partial y}]ds \\ -\overline{\Delta u_1\Delta u_i^2}+2\nu\frac{\partial}{\partial r}\overline{\Delta u_i^2}=\frac{4}{3}\overline{\varepsilon}r \end{array} \quad (2)$$

where s is a dummy variable, identifiable with the separation along x. In this paper, u_1, u_2, and u_3 will be used interchangeably with u, v, w; similarly for x_1, x_2, x_3 and x, y, z. The first and second terms on the left hand side of Eq. (2) are the large scale forcing terms which arise from the turbulent transport of $(\Delta u_i)^2$ by the mean velocity U and the lateral velocity fluctuation u_2. The third term is the generalised third-order structure function, while the fourth term represents the viscous effect. The term on the right side of Eq. (2) is proportional to the full mean energy dissipation rate and balances the sum of the other terms. Applying the limit at sufficiently large r to (2), yields the one-point kinetic energy budget, viz.

$$\frac{1}{2}U\frac{\partial\overline{q^2}}{\partial x}+\frac{\partial}{\partial y}(\frac{1}{2}\overline{u_2q^2})+\bar{\varepsilon}=0. \quad (3)$$

We first examine the conditions under which Eq. (2) satisfies similarity by assuming functional forms for the terms in this equation. Under SP hypothesis, we assume

$$\begin{array}{l} \overline{\Delta u_i^2}=u_x^2 f(\xi,\zeta), \\ -\overline{u_2\Delta u_i^2}=u_x^3 e(\xi,\zeta), \\ -\overline{\Delta u_1\Delta u_i^2}=u_x^3 g(\xi,\zeta), \end{array} \quad (4)$$

where $\xi = r/l$, $\zeta = y/\delta$; l and δ are the characteristic length scales in x and y directions, respectively; u_x is a characteristic velocity scale. The dimensionless functions $f(\xi,\zeta)$, $e(\xi,\zeta)$ and $g(\xi,\zeta)$ may depend on the ICs and are not considered here. The separation between functions of x, ξ, and ζ allows the determination of solutions to Eq. (2), for which a relative balance among all of the terms is maintained as the flow progresses downstream. After substituting Eq. (4) into Eq. (2), we obtain

$$\begin{array}{l} -\frac{U}{r^2}\frac{du_x^2}{dx}l^3\Gamma_1+\frac{Uu_x^2}{r^2}\frac{dl}{dx}l^2\Gamma_2+\frac{2u_x^3}{\delta r^2}l\Gamma_3 \\ +u_x^3 g(\xi,\zeta)+2\nu u_x^2\frac{1}{l}\frac{df(\xi,\zeta)}{d\xi}=\frac{4}{3}\overline{\varepsilon}r \end{array} \quad (5)$$

where

$$\begin{array}{l} \Gamma_1=\int_0^{r/l}\frac{s^2}{l^2}f(\xi,\zeta)d(\frac{s}{l}) \\ \Gamma_2=\int_0^{r/l}\frac{s^3}{l^3}\frac{df(\xi,\zeta)}{d\xi}d(\frac{s}{l}) \\ \Gamma_3=\int_0^{r/l}\frac{s^2}{l^2}\frac{de(\xi,\zeta)}{d\zeta}d(\frac{s}{l}) \end{array} \quad (6)$$

Note that the following relations

$$\begin{array}{l} \frac{\partial\xi}{\partial x}=-rl^{-2}\frac{dl}{dx} \\ \frac{\partial\zeta}{\partial y}=\frac{1}{l} \end{array} \quad (7)$$

have been used in deriving Eq. (5). After multiplication by $(l/\nu u_x^2)$, Eq. (5) becomes

$$\begin{array}{l} -\left[\frac{Ul^2}{\nu u_x^2}\frac{du_x^2}{dx}\right]\frac{\Gamma_1}{\xi^2}+\left[\frac{Ul}{\nu}\frac{dl}{dx}\right]\frac{\Gamma_2}{\xi^2}+[\frac{2u_xl^2}{\nu\delta}]\frac{\Gamma_3}{\xi^2} \\ +\left[\frac{u_xl}{\nu}\right]g(\xi,\zeta)+[2]\frac{df(\xi,\zeta)}{d\xi}=\left[\frac{4}{3}\frac{\overline{\varepsilon}l^2}{\nu u_x^2}\right]\xi \end{array} \quad (8)$$

Since along the centreline of the wake $U = U_\infty - U_d$, Eq. (8) can be further recast as

$$\begin{aligned} &-\left[\frac{U_\infty l^2}{\nu u_x^2}\frac{du_x^2}{dx}\right]\frac{\Gamma_1}{\xi^2}+\left[\frac{U_\infty l}{\nu}\frac{dl}{dx}\right]\frac{\Gamma_2}{\xi^2}\\ &+\left[\frac{U_d l^2}{\nu u_x^2}\frac{du_x^2}{dx}\right]\frac{\Gamma_1}{\xi^2}-\left[\frac{U_d l}{\nu}\frac{dl}{dx}\right]\frac{\Gamma_2}{\xi^2}\\ &+\left[\frac{2u_x l^2}{\nu\delta}\right]\frac{\Gamma_3}{\xi^2}+\left[\frac{u_x l}{\nu}\right]g(\xi,\zeta)\\ &+[2]\,\frac{df(\xi,\zeta)}{d\xi}=\left[\frac{4}{3}\frac{\bar{\varepsilon}l^2}{\nu u_x^2}\right]\xi \end{aligned} \tag{9}$$

For equilibrium similarity, all the terms within square brackets must evolve in the streamwise direction in exactly the same way. Since the last term on the left hand side of Eq. (8) is constant, all the other terms must also be constant, viz.

$$\frac{U_\infty l^2}{\nu u_x^2}\frac{du_x^2}{dx} = C_1, \tag{10}$$

$$\frac{U_\infty l}{\nu}\frac{dl}{dx} = C_2, \tag{11}$$

$$\frac{U_d l^2}{\nu u_x^2}\frac{du_x^2}{dx} = C_3, \tag{12}$$

$$\frac{U_d l}{\nu}\frac{dl}{dx} = C_4, \tag{13}$$

$$\frac{u_x l^2}{\nu\delta} = C_5, \tag{14}$$

$$\frac{u_x l}{\nu} = C_6, \tag{15}$$

$$\frac{\bar{\varepsilon}l^2}{\nu u_x^2} = C_7. \tag{16}$$

Eq. (15) indicates that in the far-wake of a cylinder, the Reynolds numbers, based on the characteristic length and velocity scales (u_x and l), must remain constant if SP is achieved but not necessarily infinite.

The ratios of Eq. (12) to Eq. (10) and Eq. (13) to Eq. (11) lead to

$$\frac{C_3}{C_1} = \frac{C_4}{C_2} = \frac{U_d}{U_\infty}. \tag{17}$$

i.e. U_d/U_∞ must be constant for exact SP. Since U_d decreases as x/d increases, one expects that beyond a certain value of x/d, $U_d/U_\infty \simeq 0$ so that SP may be satisfied approximately i.e. C_3 and C_4 are negligible compared to C_1 and C_2.

Then, from Eq. (11), the characteristic length scale should behave as

$$\frac{l}{d} = c_1\left(\frac{x}{d}-\frac{x_0}{d}\right)^{1/2} \tag{18}$$

where x_0 is the effective flow origin, c_1 is the power-law prefactors for l.

Eq. (10) and Eq. (16) suggests that u_x and $\bar{\varepsilon}$ should behave as

$$\frac{u_x}{U_\infty} = c_2\left(\frac{x}{d}-\frac{x_0}{d}\right)^{1/2} \tag{19}$$

$$\frac{\overline{\varepsilon}d}{U_\infty^3} = c_\varepsilon\left(\frac{x}{d}-\frac{x_0}{d}\right)^{-2} \tag{20}$$

Note that Eq. (18), Eq. (19) and Eq. (20) have been normalized by d and U_∞. Combining (14) and (15) shows that the characteristic length scale δ in y direction should behave like l, viz.

$$\frac{\delta}{l} = const \tag{21}$$

which explicitly predicts that the half-width of the far-wake L_0 should behave like $(x-x_0)^{1/2}$.

More importantly, an exact equation to estimate $\bar{\varepsilon}$ can be derived from the present SP analysis. To this end, we focus on the transport equation for the mean turbulent kinetic energy ($\overline{q^2} = \overline{u_i^2}$) along the axis of the far-wake, i.e. Eq. (3).

Several attempts have been made to measure the various terms of Eq. (3) in a circular cylinder. For example, Browne *et al.* (1987), Aronson & Löfdahl (1993), and Lefeuvre *et al.* (2014) showed that, on the centreline of a circular cylinder, the advection (the first term in Eq. (3)) and diffusion (the second term in Eq. (3)) terms contribute significantly to the budget (the ratio of the diffusion term to advection term is about 1). Thus, to quantify the power-law prefactors c_1, c_2, and c_ε and their interrelationships in Eq. (18) and Eq. (19), we assume

$$\frac{\partial\overline{vq^2}}{\partial y} \approx U\frac{\partial\overline{q^2}}{\partial x} \tag{22}$$

Eq. (3) then can be rewritten as

$$U\frac{\partial\overline{q^2}}{\partial x} + \bar{\varepsilon} \approx 0. \tag{23}$$

The turbulent kinetic energy along the axis of the far-wake is approximated by

$$\overline{q^2} = \overline{u_1^2} + 2\overline{u_2^2} = \overline{u_1^2}(1+2R) \tag{24}$$

where $R = \overline{u_2^2}/\overline{u_1^2}$, and accounts for large-scale anisotropy.

After substituting Eq. (20) and Eq. (24) in Eq. (23), we obtain

$$\frac{\overline{u^2}}{U_\infty^2} = \frac{c_\varepsilon}{(1+2R)}\left(\frac{x-x_0}{d}\right)^{-1} = A_u^2\left(\frac{x-x_0}{d}\right)^{-1} \tag{25}$$

where A_u is a power-law prefactor for u'.

Note that the condition that U_d/U_∞ is negligible (see Eq. (17)) is used in deriving Eq. (25).

We recall that a reliable estimation of the energy dissipation rate is a challenging task for the experimentalist.

Eq. (25) provides a simple means for estimating $\bar{\varepsilon}$ along the wake axis once $\overline{u^2}$ and R are known, viz.

$$\frac{\overline{\varepsilon}d}{U_\infty^3} = c_\varepsilon(\frac{x}{d}-\frac{x_0}{d})^{-2} = A_u^2(1+2R)(\frac{x}{d}-\frac{x_0}{d})^{-2} \quad (26)$$

It should be noted that there is an anisotropy in the far wake of a circular cylinder, even on the flow centreline where the mean shear is zero (e.g. Browne *et al.*, 1987; Antonia & Browne, 1986). The departure from local isotropy is quantified directly by

$$R_\varepsilon = \frac{\bar{\varepsilon}_{iso}}{\bar{\varepsilon}} \quad (27)$$

Thus, the isotropic energy dissipation rate $\overline{\varepsilon}_{iso}$ is given by

$$\frac{\overline{\varepsilon}_{iso}d}{U_\infty^3} = A_u^2 R_\varepsilon(1+2R)(\frac{x}{d}-\frac{x_0}{d})^{-2} \quad (28)$$

It follows that the Kolmogorov scales should behave as

$$\frac{u_K}{U_\infty} = \left[\frac{A_u^2 R_\varepsilon(1+2R)}{\mathrm{R}_d}\right]^{1/4}(\frac{x}{d}-\frac{x_0}{d})^{-1/2} \quad (29)$$

$$\frac{\eta}{d} = \left[\mathrm{R}_d^3 R_\varepsilon A_u^2(1+2R)\right]^{-1/4}(\frac{x}{d}-\frac{x_0}{d})^{1/2} \quad (30)$$

and therefore

$$\overline{u^{*2}} = \frac{\overline{u^2}}{u_K^2} = [\frac{A_u^2 \mathrm{R}_d}{(1+2R)R_\varepsilon}]^{1/2} \quad (31)$$

is constant, independently of x.

Since $\overline{u^{*2}} = R_\lambda/\sqrt{15}$, it follows that

$$A_{R_\lambda} = \frac{R_\lambda}{\mathrm{R}_d{}^{1/2}} = [\frac{15A_u^2}{(1+2R)R_\varepsilon}]^{1/2} \quad (32)$$

The definition of the Taylor microscale leads to

$$\frac{\lambda^2}{d^2} = \frac{15\nu\overline{u^2}}{\overline{\varepsilon}_{iso}d^2} = \frac{15}{\mathrm{R}_d(1+2R)R_\varepsilon}(\frac{x}{d}-\frac{x_0}{d}). \quad (33)$$

And the ratio λ/η

$$\lambda^* = \frac{\lambda}{\eta} = \left[\frac{15^2 \mathrm{R}_d A_u^2}{(1+2R)R_\varepsilon}\right]^{1/4} \quad (34)$$

The present equilibrium similarity analysis leads to an exact expression for $\overline{u}^2$, $\overline{\varepsilon}$ and all subsequent quantities. In particular, the relationships between the prefactors A_u, A_{R_λ}, and c_ε are provided. All the results derived from the equilibrium similarity in the far-wake are tested in the next section.

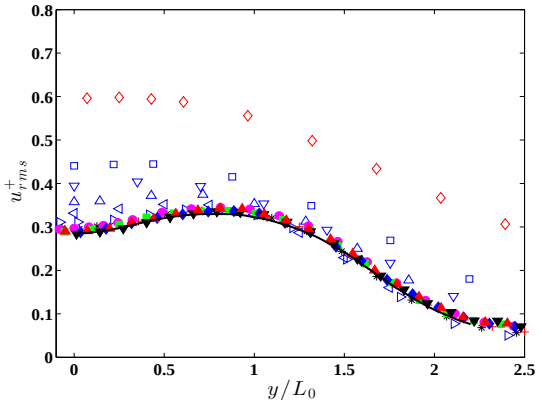

Figure 2. Normalized rms longitudinal velocity at $R_d = 2000$. ◇, $x/d = 20$; ❑, 40; ▽, 60; △, 80; ◁, 100; ▷, 170; ∗, 211; ●, 277; ●, 344; ■, 401; ◆, 468; ▼, 534; ▲, 601. Solid curve corresponds to the cylinder far-wake at $x/d = 420$ (Browne *et al.*, 1987).

Results

The root mean square of the streamwise fluctuations u^+_{rms}, normalised with U_d and L_0 are shown in Fig. 2. Antonia & Mi (1998) reported that the magnitude of u^+_{rms} decreases as x/d increases over the range $x/d = 10 \sim 70$. The same can be observed in Fig. 2. More importantly, the magnitude of u^+_{rms} keeps decreasing as x/d increases, eventually reaching a constant beyond $x/d \approx 200$. This suggests SP is satisfied closely for $x/d > 200$, at least in the context of Reynolds stresses.

From the SP analysis, we show that the Reynolds numbers, based on any characteristic set of length and velocity scales, must remain constant in the far-wake if SP is satisfied. The local Reynolds number $R_0 = U_d L_0/\nu$, defined on the basis of the scaling parameters: L_0 and U_d, and the Taylor microscale Reynolds number R_λ are shown in Fig. 3. As expected, both the R_0 and R_λ become constant for $x/d > 200$ implying that SP is satisfied closely. Although not shown here, we have checked that the length-scales (namely, the integral scale, L_0, the Taylor microscale, and the Kolmogorov scale) grow as $x^{1/2}$ and the velocity scales (namely, U_d, the u', the Kolmogorov velocity scale) decay as $x^{-1/2}$ for $x/d > 200$, in agreement with the consequences of the SP analysis i.e. Eqs. (18) and (19).

Eq. (26) provides a simple means for estimating $\bar{\varepsilon}$ along the wake axis once $\overline{u^2}$ and R are known. Before checking the accuracy of the present estimates for $\bar{\varepsilon}$ with Eq. (26), we first used a spectral chart method to estimate $\bar{\varepsilon}$ (Djenidi & Antonia, 2012). This method is based on the validity of the first similarity hypothesis of Kolmogorov (1941) (or $K41$) which implies that spectra of velocity fluctuations scale on ν and $\bar{\varepsilon}$ at large Reynolds numbers. However, Antonia *et al.* (2014) pointed out that the collapse of the turbulent dissipative range on Kolmogorov scales does not require either of the two major assumptions in $K41$, viz. R_λ should be very large and local isotropy must be valid. Antonia *et al.* (2014) showed that a similarity solution of the small-scale motions based on u_K and η remains plausible provided the large scale inhomogeneity in the K-H equation is small with respect to the term containing $\overline{\varepsilon}$ and ν. Kolmogorov normalization breaks down only when R_λ falls below a value of about 20 (Djenidi *et al.*, 2014). The ro-

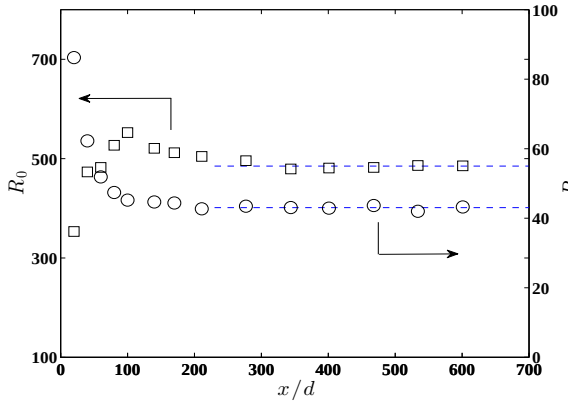

Figure 3. Downstream evolution for R_λ (◯) and R_0 (❑). Dashed lines indicate the mean values for each plotted quantity over the range $x/d = 200 \sim 600$.

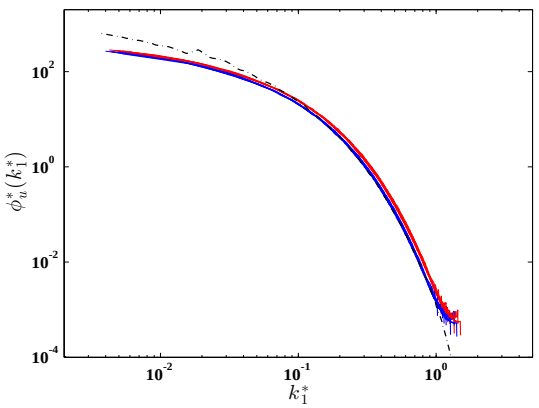

Figure 4. Spectra of the turbulent energy u^2 over the range $x/d = 200 \sim 600$. The red curves are normalised by $\bar{\varepsilon}_{iso}$ and ν, while the blue curves are normalised by $\bar{\varepsilon}_{spec}$ (based on the spectral chart method) and ν. The black curve corresponds to the spectrum on the centreline of a fully developed channel flow (Abe *et al.*, 2009).

bustness of the collapse of the normalised one-dimensional spectra $\phi_u^*(k_1^*)$ at sufficiently large k_1^* underpins the estimates of $\bar{\varepsilon}$ in the far-wake where $R_\lambda \simeq 43$ (see Fig. 3). Fig. 4 shows the distributions of $\phi_u^*(k_1^*)$ for several positions over the range $200 < x/d < 600$. The red curves are normalised by $\bar{\varepsilon}_{iso}$ and ν, while the blue curves are normalised by $\bar{\varepsilon}_{spec}$ (based on the spectral chart method) and ν. Also for reference, the velocity spectrum on the centreline of a fully developed channel flow is shown (Abe *et al.*, 2009). There is a very good agreement between the blue curves and the channel flow spectrum. On the other hand, the spectra normalised by $\bar{\varepsilon}_{iso}$ and ν are shifted up, suggesting that $\bar{\varepsilon}_{iso}$ differs from the actual $\bar{\varepsilon}$ ($\simeq \bar{\varepsilon}_{spec}$). In this case, the relation $R_\varepsilon = \bar{\varepsilon}_{iso}/\bar{\varepsilon}_{spec}$ is 0.78.

We recall that Browne *et al.* (1987); Antonia & Browne (1986) measured all components of $\overline{\varepsilon}$ at R_d=1170. They showed R_ε=2/3, which is smaller than the present value of 0.78 at $R_d = 2000$. Arguably, R_ε will become 1 at sufficiently large Reynolds number. We believe this difference is due to the Reynolds number effects since we also used the spectral chart method to estimate R_ε at R_d=1000 (not shown). The resulting value is R_ε=0.66, which is exactly the same as the measured value by Browne *et al.* (1987); Antonia & Browne (1986) at R_d=1170.

Now, we estimate $\bar{\varepsilon}$ with Eq. (26). At $R_d = 2000$, Hao *et al.* (2008) showed that both $\overline{u_1^2}/\overline{u_2^2}$ and $\overline{u_1^2}/\overline{u_3^2}$ are about 1.4 on the centreline of the far-wake. Namely $R = 0.71$ at $R_d = 2000$. Estimates of $\bar{\varepsilon}$ from Eq. (26) are shown in Fig. 5 with $A_u = 0.318$, $x_0 = 25d$, and $R = 0.71$ (A_u and x_0 are estimated from the present data). Also shown are the isotropic energy dissipation rate $\bar{\varepsilon}_{iso}$. Estimated R_ε from this figure is 0.75 (the square symbols for $\bar{\varepsilon}_{iso}$/0.75 collapses reasonably well with the $\bar{\varepsilon}$), which is in good agreement with the estimate from the spectral chart method above, validating that Eq. (26) has estimated $\bar{\varepsilon}$ correctly.

In addition, the predicted value for A_{R_λ} from Eq. (32) is 0.92 which is also in agreement with the experimental value of 0.96 at $R_d = 2000$. Since, as noted in the Introduction, there is abundant evidence to indicate that the SP depends on the ICs, the ratio A_{R_λ}, A_u, and c_ε should also depend on the ICs. Indeed, as pointed out by Antonia *et al.* (2002), although the ratio A_{R_λ} (or $R_\lambda/R_d^{1/2}$) is approximately independent of R_λ at $x/d = 70$ in wakes generated

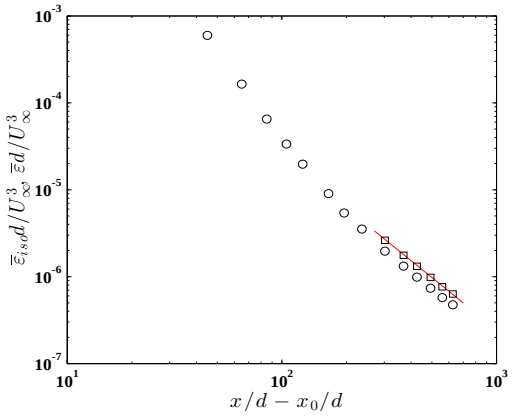

Figure 5. Downstream evolution of $\bar{\varepsilon}$ (red line, calculated from Eq. (26) with $A_u = 0.318$, $x_0 = 25d$, and $R = 0.71$); experimental data, $\bar{\varepsilon}_{iso}$ (◯); and $\bar{\varepsilon}_{iso}$/0.75 (❑).

by five different bluff bodies, i.e. a solid circular cylinder, a circular cylinder constructed from a screen of 54% solidity, a solid square cylinder, a solid plate placed normal to the flow, and screen strip, over a range of Reynolds numbers, its magnitude varies significantly between these different wakes at same R_d.

Conclusions

Traditional arguments indicate that the mean velocity defect and Reynolds stress profiles in the far-wake should exhibit an approximate SP behaviour although the influence of the ICs cannot ruled out, as indicated by George (2012). Many analyses of single-point statistical moments (i.e. Eq. (1)) have been reported for the far-wake in previous investigations. In this paper, we extend the SP analysis to two-point statistics, i.e. an SP analysis of the scale-by-scale energy budget equation. There are three major conclusions which arise from this work. (i) The power-law variations for the different length-scales (namely, the integral scale, L_0, the Taylor microscale, and the Kolmogorov length scale)

and the velocity scales (namely, U_d, u', the Kolmogorov velocity scale) are derived. (ii) From the SP analysis, we show that the Reynolds number: R_0 and R_λ , based on the characteristic length and velocity scales, remain constant in the far-wake where SP is achieved approximately. (iii) an exact relation for estimating the evolution of the mean turbulent energy dissipation rate $\bar{\varepsilon}$ alone the axis is obtained. All the above results are supported reasonably well by the hot-wire data in the far-wake of a circular cylinder.

The financial support by the Australian Research Council is acknowledged.

REFERENCES

Abe, H., Antonia, R. A. & Kawamura, H. 2009 Correlation between small-scale velocity and scalar fluctuations in a turbulent channel flow. *J. Fluid Mech.* **627**, 1–32.

Anselmet, Gagne, Y., Hopfinger, E. J. & Antonia, R. A. 1984 Higher-order velocity structure functions in turbulent shear flows. *J. Fluid Mech.* **140**, 63–89.

Antonia, R . A ., Browne, L . W . B ., Bisset, D . K . & Fulachier, L . 1987 A description of the organized motion in the turbulent far wake of a cylinder at low Reynolds number. *J. Fluid Mech.* **184**, 423–444.

Antonia, R. A. & Browne, L. W. 1986 Anisotropy of temperature dissipation in a turbulent wake. *J. Fluid Mech.* **163**, 393–403.

Antonia, R. A., Browne, L. W. B. & Shah, D. A. 1988 Characteristics of vorticity fluctuations in a turbulent wake. *J. Fluid Mech.* **189**, 349–365.

Antonia, R. A., Djenidi, L. & Danaila, L. 2014 Collapse of the turbulent dissipation range on Kolmogorov scales. *Phys. Fluids* **26**, 045105.

Antonia, R. A. & Mi, J. 1998 Approach towards self-preservation of turbulent cylinder and screen wakes. *Experimental Thermal and Fluid Science* **17**, 277–284.

Antonia, R. A., Zhou, T. & Romano, G. P. 2002 Small-scale turbulence characteristics of two-dimensional bluff body wakes. *J. Fluid Mech.* **459**, 67–92.

Aronson, D. & Löfdahl, L. 1993 The plane wake of a cylinder: Measurements and inferences on turbulence modeling. *Phys. Fluids* **5**, 1433.

Bisset, D. K., Antonia, R. A. & Britz, D. 1990b Structure of large-scale vorticity in a turbulent far wake. *J. Fluid Mech.* **218**, 463–482.

Bisset, D. K., Antonia, R. A. & Browne, L. W . B. 1990a Spatial organization of large structures in the turbulent far wake of a cylinder. *J. Fluid Mech.* **218**, 439–461.

Brown, G. L. & Roshko, A. 2012 Turbulent shear layers and wakes. *Journal of Turbulence* **13**, 1–32.

Browne, L. W., Antonia, R. A. & Shah, D. A. 1987 Turbulent energy dissipation in a wake. *J. Fluid Mech.* **179**, 307–326.

Browne, L. W. B. & Antonia, R. A. 1986 Reynolds shear stress and heat flux measurements in a cylinder wake. *Phys. Fluids* **29**, 709.

Burattini, P., Antonia, R. A. & Danaila, L. 2005 Similarity in the far field of a turbulent round jet. *Phys. Fluids* **17**, 025101.

Camussi, R. & Guj, G. 1995 Experimental analysis of scaling laws in low and moderate Re grid generated turbulence. *Exp. Fluids* **24**, 63–67.

Danaila, L., Anselmet, F., Zhou, T. & Antonia, R. A. 2001 Turbulent energy scale-budget equations in a fully developed channel flow. *J. Fluid Mech.* **430**, 87–109.

Djenidi, L. & Antonia, R. A. 2012 A spectral chart method for estimating the mean turbulent kinetic energy dissipation rate. *Exp. Fluids* **53**, 1005–1013.

Djenidi, L., Tardu, S.F., Antonia, R.A. & Danaila, L. 2014 Breakdown of Kolmogorov's first similarity hypothesis in grid turbulence. *Journal of Turbulence* **15**, 596–610.

George, W. K. 1989 The self-preservation of the turbulent flows and its relation to initial conditions and coherent structures, in w. k. george and r. arndt (eds.). *Advances in Turbulence, Berlin, Springer* pp. 39–74.

George, W. K. 2012 Asymptotic effect of initial and upstream conditions on turbulence. *J. Fluids Eng.* **134**, 061203.

Hao, Z., Zhou, T., Chua, L. P. & Yu, S. C. M. 2008 Approximations to energy and temperature dissipation rates in the far field of a cylinder wake. *Experimental Thermal and Fluid Science* **32**, 791–799.

Kolmogorov, A. 1941 Dissipation of energy in the locally isotropic turbulence. *Dokl. Akad. Nauk SSSR* **125**, 15–17.

Lefeuvre, N., Djenid, L., Antonia, R. A. & Zhou, T. 2014 Turbulent kinetic energy and temperature variance budgets in the far-wake generated by a circular cylinder. *19th Australasian Fluid Mechanics Conference* .

Thiesset, F., Antonia, R. A. & Djenidi, L. 2014 Consequences of self-preservation on the axis of a turbulent round jet. *J. Fluid Mech.* **748** (R2).

Townsend, A. A. 1956 *The Structure of turbulent shear flow, 1st ed.*. Cambridge University Press.

Wygnanski, I., Champagne, F. & Marasli, B. 1986 On the large-scale structures in two-dimensional, small-deficit, turbulent wakes. *J. Fluid Mech.* **168**, 31–71.

Zhou, T., Hao, Z., Chua, L. P. & Zhou, Y. 2006 Comparisons between different approximations to energy dissipation rate in a self-preserving far wake. *Physical Review E* **74**, 056308.

Zhou, Y. & Antonia, R. A. 1995 Memory effects in a turbulent plane wake. *Exp. Fluids* **19**, 112–120.

Zhou, Y., Antonia, R. A. & Tsang, W. K. 1998 The effect of Reynolds number on a turbulent far-wake. *Exp. Fluids* **25**, 118–125.